Science of the Total Environment 865 (2023) 161119

Contents lists available at ScienceDirect

Science of the Total Environment

journal homepage: www.elsevier.com/locate/scitotenv

Projected mid-century rainfall erosivity under climate change over the southeastern United States

Bijoychandra S. Takhellambam [a,*], Puneet Srivastava [b], Jasmeet Lamba [a,*], Ryan P. McGehee [c], Hemendra Kumar [a,d], Di Tian [e]

[a] Auburn University, Department of Biosystem Engineering, 350 Mell St, Auburn, AL 36849, USA
[b] University of Maryland, Agricultural Experiment Station, Symons Hall, 7998 Regents Drive, College Park, MD 20742, USA
[c] Purdue University, Agricultural and Biological Engineering, 225 South University Street, West Lafayette, IN 47907, USA
[d] The Ohio State University, School of Environment and Natural Resources, 2021 Coffey Rd, Columbus, OH 43210, USA
[e] Auburn University, Department of Crop, Soil and Environmental Sciences, 201 Funchess Hall, AL 36849, USA

HIGHLIGHTS

- Projected future (2030–2059) R-factor using downscaled 15-min precipitation data.
- Erosivity was quantified using RUSLE2 energy equation without data limitations.
- Future ensemble mean annual R-factor is project to increase by 47 % from historical.
- Much of the increase in R-factor can be attributed to increase in intensity.

GRAPHICAL ABSTRACT

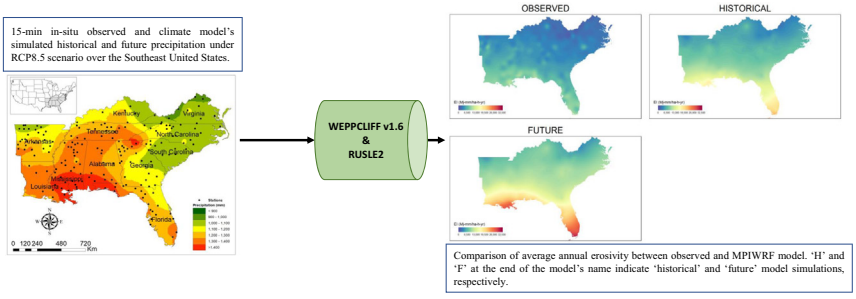

ARTICLE INFO

Editor: Manuel Esteban Lucas-Borja

Keywords:
Erosion index
RUSLE2
Soil Erosion
15-min rainfall
CMIP5
Temporal downscaling

ABSTRACT

Recent observations and climate change projections indicate that changes in rainfall energy, intensity, duration, and frequency, which determine the erosive power of rainfall, will amplify erosion rates around the world. However, the magnitude and scope of these future changes in erosive power of rainfall remain largely unknown, particularly at finer-resolutions and local scales. Due to a lack of available projected future sub-hourly climate data, previous studies relied on aggregates (hourly, daily) rainfall data. The erosivity for the southeastern United States in this study was calculated using the RUSLE2 erosivity calculation method without data limitation and a recently published 15-min precipitation dataset. This precipitation data was derived from five NA-CORDEX climate models' precipitation products under the Representative Concentration Pathway (RCP) 8.5 scenario. In this dataset, hourly climate projections of precipitation were bias-corrected and temporally downscaled to 15-min resolution for 187 locations with collocated 15-min precipitation observations. Precipitation, erosivity (R-factor), and erosivity density (ED) estimations were provided for historical (1970–1999) and future (2030–2059) time periods. Ensemble results for projected values (as compared to historical values) showed increase in precipitation, erosivity, and erosivity density by 14 %, 47 %, and 29 %, respectively. The future ensemble model showed an average annual R-factor of 11,237 ± 1299 MJ mm $ha^{-1}h^{-1}yr^{-1}$. These findings suggest that changes in rainfall intensity, rather than precipitation amount, may be driving the change in erosivity. However, the bias correction and downscaling limitations inherent in the original precipitation dataset and this study's analyses obscured this particular result. In general, coastal and mountainous regions

Abbreviations: BC, Bias correction; COV, Coefficient of variation; DS, Downscaling; e, Rainfall kinetic energy per unit depth; ED, Erosivity density; E_s, Storm erosivity; F, Future; H, historical; h, hour; ha, hectare; I, Intensity; Max., Maximum; Med., Median; Min., minimum; min, minute; MJ, Megajoule; mm, millimeter; Obs.Abs.Diff., Observed absolute difference; Obs.Rel.Diff., Observed relative difference; R or R-factor, Annual Rainfall Erosivity; RCP, Representative Concentration Pathway; R2 or RUSLE2, Revised Universal Soil Loss Equation 2; Sim.Abs.Diff., Simulated absolute difference; Sim.Rel.Diff., Simulated relative difference; Std.Dev., Standard deviation.

* Corresponding authors.
E-mail addresses: tzs0075@auburn.edu (B.S. Takhellambam), jsl0005@auburn.edu (J. Lamba).

http://dx.doi.org/10.1016/j.scitotenv.2022.161119
Received 5 May 2022; Received in revised form 6 December 2022; Accepted 18 December 2022
Available online 27 December 2022

are expected to experience the greatest absolute increase in erosivity, while other inland areas are expected to experience the greatest relative change. This study offers a novel examination of projected future precipitation characteristics in terms of erosivity and potential future erosion.

1. Introduction

According to the United Nations Food and Agriculture Organization, soil erosion has been reported as one of the greatest challenges for sustainable soil management (FAO et al., 2019; Grillakis et al., 2020). Soil erosion has a severe impact on the land productivity, water bodies, and socioeconomics of a region (Almagro et al., 2017; Biasutti and Seager, 2015). During soil erosion events, nutrients and organic matter are carried away through runoff which reduces soil fertility, effective root depth, and negatively impacts water quality by increasing turbidity of surface waters (Biasutti and Seager, 2015; Segura et al., 2014). Globally, soil erosion has reduced both cropland area and crop yield at rates of 10 million ha (Grillakis et al., 2020; Pimentel, 2006) and 0.4 % every year, respectively (FAO et al., 2019), resulting in an annual economic loss of $400 billion (Borrelli et al., 2017).

Among various drivers causing soil erosion (i.e., water, wind, change in land use, and cultivation practices) (Borrelli et al., 2017; Naipal et al., 2018; Webb et al., 2017), water is considered the primary natural cause of soil erosion through both rainfall and runoff processes (Cerdà et al., 2009). The potential of rainfall to erode soil or rainfall erosivity is a function of both rainfall kinetic energy and maximum 30-min rainfall intensity (McGehee and Srivastava, 2018; Renard, 1997; Wischmeier and Smith, 1978, 1965, 1958). Characteristics of rainfall mostly responsible for changes in erosivity include energy, intensity, frequency, and duration (McGehee, 2016; McGehee and Srivastava, 2018). Climate change is projected to alter the rainfall characteristics due to increases in atmospheric specific humidity, warmer climate, and seasonal rainfall (Konapala et al., 2020; Panagos et al., 2022). This will likely increase the extreme rainfall events and may act as one of the main drivers for increasing land degradation, loss of agricultural productivity, as well as soil erosion (Borrelli et al., 2021).

The effects of climate change on extreme precipitation events (>50.8 mm in a day) in the United States have been observed since 1910 (Karl et al., 1996; Pruski and Nearing, 2002). The frequency of extreme precipitation events has increased more than the average number of events in the last three decades. In a similar way, the Southeast United States has also recorded historically the highest number of daily extreme rainfalls with 76.2 mm or more during the decadal periods of the 1990s, 2000s, and 2010s, with 1st, 3rd, and 2nd highest number of rainfall events, respectively (USGCRP, 2018). Extreme events have increased during these time periods of the 1990s, 2000s, and 2010 by 23 %, 16 %, and 20 %, respectively, compared to the estimated average of 0.95 days per year in the 1900s.

According to the Intergovernmental Panel on Climate Change (IPCC, 2018), temperature at the end of 2052 is likely to increase by 1.5 °C from pre-industrial levels with the current rate of greenhouse gas emission. This will affect the precipitation characteristics; for instance, intensity is expected to increase up to 7 % for each 1 °C increase in temperature (Easterling et al., 2017). Precipitation in the Southeast United States is anticipated to increase in all seasons except summer. The decrease in precipitation in summer could be as high as 15 % in parts of Arkansas, Louisiana, and South Florida (Ingram et al., 2013; Keim et al., 2011). Therefore, climate change will affect future precipitation characteristics, thereby increasing the complexity of precipitation patterns of intensity, amount, duration and frequency (Almagro et al., 2017; Pruski and Nearing, 2002; Seager et al., 2009).

Rainfall erosivity of the Southeast United States may be more susceptible to climate change than other parts of the country owing to the extensive range of erosivity (2000 to >10,000 MJ mm $ha^{-1}h^{-1}yr^{-1}$) and high intensities in lower latitudes (Kunkel et al., 2013; McGehee, 2016; McGehee and Srivastava, 2018; Trenberth et al., 2003). Therefore, quantifying projected changes in rainfall erosivity for the southeastern US will be key for strategic identification of regions prone to soil erosion.

The estimation of erosivity can be categorized mainly in two approaches based on the temporal scale of rainfall data i.e., i) high resolution rainfall data and ii) aggregated (hourly, daily or monthly) rainfall data (see Supplementary Table S1 for their pros and cons) (Fischer et al., 2018; McGehee, 2016; McGehee and Srivastava, 2018; McGehee et al., 2022). Previous erosion maps, especially those of three Agricultural Handbooks (AH) i.e., AH282 (Wischmeier and Smith, 1965), AH537 (Wischmeier and Smith, 1978) and AH703 (Renard, 1997), were found to be about 30 % lower than the same erosivity values from benchmarking studies (McGehee, 2016; McGehee and Srivastava, 2018; McGregor et al., 1995). Considering the discrepancies, McGehee (2016) recommended a better procedure for generating erosivity maps from 15-min data, which was more consistent with breakpoint precipitation observations from McGregor et al. (1995) and the original erosivity work by Wischmeier and Smith (1958). The term “breakpoint” data refer to precipitation data that are measured using “breaks” in rainfall characteristics such as intensity. This should not be confused with “breakpoint format” data, which could be derived from any precipitation measurements and represented with “breaks” that do not necessarily preserve precipitation characteristics. So, breakpoint data rainfall characteristics are preserved within the level of gauge's accuracy and precision (McGehee et al., 2021). McGehee and Srivastava (2018) used non-breakpoint, 15-min precipitation data to estimate rainfall erosivity (R-factor) in the Southeast US for the period 1970–2013. They validated their approach using breakpoint data from McGregor et al. (1995) after making proper adjustments or corrections to account for differences between the two data types. Therefore, with proper accounting, it is possible to approximate breakpoint erosivity using 15-min, fixed-interval precipitation data.

It is important to determine how future erosivity values may change in response to climate change. There have been numerous previous works on the estimation of rainfall erosivity around the world (Almagro et al., 2017; Ballabio et al., 2017; Beguería et al., 2018; Bonilla and Vidal, 2011; Grillakis et al., 2020; Meusburger et al., 2012; Mondal et al., 2016; Nyssen et al., 2005; Panagos et al., 2022; Riquetti et al., 2020; Shiono et al., 2013; Zhang et al., 2010). However, to our knowledge, only a few have studied projected erosivity in the United States (Biasutti and Seager, 2015; Hoomehr et al., 2016; Nearing, 2001; Panagos et al., 2022; Segura et al., 2014). Nearing (2001) used the erosivity method developed by Renard and Freimund (1994) that relies upon both monthly rainfall and annual rainfall amounts from two coupled atmospheric ocean Global Circulation Model (GCM). Biasutti and Seager (2015) used a statistical relationship between daily precipitation and rainfall erosivity. The relationship between 20 years (1981–2000) of observed precipitation and erosivity was developed and subsequently applied for future scenarios at both daily and monthly time scales. Hoomehr et al. (2016) investigated the future daily rainfall erosivity for 2010–2099 under three climate scenarios (A1F1, A1B, and B1) using monthly precipitation for the southern Appalachian region of the US. Panagos et al. (2022) used a regression model known as Gaussian Process Regression for the estimation of projected rainfall erosivity around the globe for 2041–2060 and 2061–2080. The model used a relationship between the rainfall erosivity and monthly climatic variables of average rainfall depth, maxima and minima of temperature, and 19 bioclimatic variables from WorldClim (Fick and Hijmans, 2017; Panagos et al., 2017).The prior studies' results were based on aggregated precipitation data (e.g., daily, monthly precipitation) or statistical

relationships, and therefore, they obscure the effects of rainfall intensity, especially smoothing of intensity, which are critical for erosivity calculation (Fischer et al., 2018; Flanagan et al., 2020; Hollinger et al., 2002; McGehee et al., 2022).

To-date, studies of erosivity derived from projected precipitation data have been limited by a lack of projected sub-hourly precipitation data comparable to the breakpoint precipitation data used in its original discovery (Wischmeier and Smith, 1958). Recent research has tentatively confirmed that fixed-interval data of about 5-min resolution is roughly equivalent to breakpoint data in the few locations those data products have been compared (Flanagan et al., 2020; Hollinger et al., 2002). The equivalent fixed-interval resolution could be slightly different for other locations. The single greatest limiting factor in studies of future erosivity is the resolution of even dynamically-downscaled climate data from GCM- Regional Circulation Models (RCM), which is currently available at hourly resolutions. Takhellambam et al. (2022) further downscaled hourly climate projection data to 15-min resolution for several climate models at 187 locations with matching observed data over the Southeast United States. Though this data is subject to underestimation biases for erosivity (Takhellambam et al., 2022), it is still one of the best options presently available for an analysis of future erosivity. Therefore, the objective of our study is to estimate the future (2030–59) rainfall erosivity using temporally downscaled 15-min rainfall datasets over the Southeast Unites States. Moreover, the projected future values will be compared to historical (1970–1999) values and historical values to observed values to inform the interpretation of the results.

2. Material and methods

Precipitation data from observed station data and GCM-RCM historical and projected future simulations were acquired and pre-processed for subsequent erosivity calculations and comparisons. Relevant procedures for acquiring and pre-processing the original precipitation data and for calculating erosivity and erosivity density values are provided below.

2.1. Data and study area

The area of interest for this study includes southeastern states of Alabama, Arkansas, Florida, Georgia, Kentucky, Louisiana, Mississippi, North Carolina, South Carolina, Tennessee, and Virginia (Fig. 1). The region receives annual rainfall of 1000–1250 mm on average in inland areas and can receive up to 1500 mm near the coastline, which are both above the average annual rainfall for the contiguous US of 856 mm (Ingram et al., 2013; Kumar et al., 2022b, 2022a, 2021). A warming climate is likely to bring more frequent extreme climates (Allan and Soden, 2008; Easterling et al., 2017). In addition, higher frequencies of rainfall intensities, especially in the lower altitudes are observed due to disproportionate moisture convergence. Moreover, the Gulf of Mexico and the Atlantic Ocean play a key role in distinguishing this region's climate from rest of the country (Ingram et al., 2013; Kunkel et al., 2013).

Observed 15-min precipitation data (DSI-3260) from 1970 to 2013 was obtained from the National Oceanic and Atmospheric Administration (NOAA NCEI, 2014). The data were post-processed from raw tape format by McGehee and Srivastava (2018). This data was quality checked and gap-filled by McGehee et al. (2022) who used WEPPCLIFF, which is a command-line tool to process climate inputs for soil loss models. This should not be confused with erosivity calculations which were performed for this study using the same tool and is discussed more later. The quality checked and gap-filled data from McGehee et al. (2022) was provided to Takhellambam et al. (2022) who filtered the datasets to 187 stations (Fig. 1) using 20.11 screening method provided by McGehee and Srivastava (2018). The 20.11 screening method means that a given station to pass screening requires at least 20 years of measured precipitation data with at least 11 months of complete observations per year.

Historical and projected future precipitation data was acquired for five different RCM-GCMs (Table 1) hourly products with a spatial resolution of approximately 50 km × 50 km in the North American Coordinated Regional Climate Downscaling Experiment (NA-CORDEX). We choose these models owing to the highest available temporal resolution of 1-h for future scenarios. Moreover, the representative concentration pathway

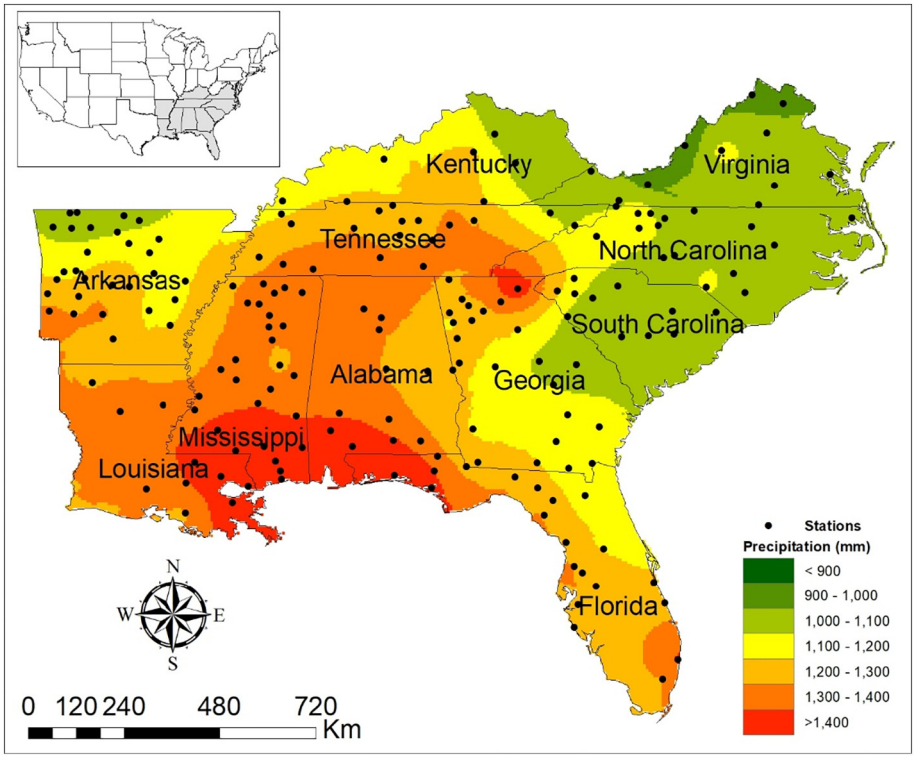

Fig. 1. Map showing the spatial distribution of observed (1970–2013) average annual precipitation with 187 precipitation stations over the Southeast United States.

Table 1
Climate models used in this study.

Acronym	GCM	RCM	References
CANESM2_CANRCM4	Canadian Earth System Model	Canadian Regional Climate Model version 4	Scinocca et al., 2016
HadGEM2-ES.WRF	Hadley Centre Global Environment Model version 2 Earth system model	Weather Research and Forecasting	Skamarock et al., 2005
GFDL-ESM2M.WRF	Earth System Model – Geophysical Fluid Dynamics Laboratory	Weather Research and Forecasting	Skamarock et al., 2005
MPI-ESM-LR. RegCM4	Max Planck Institute for Meteorology Earth System Model LR	Regional Climate Model version 4	Giorgi and Anyah, 2012
MPI-ESM-LR.WRF	Max Planck Institute for Meteorology Earth System Model LR	Weather Research and Forecasting	Skamarock et al., 2005

(RCP8.5) represents the most pessimistic or worst-case emissions scenario which would be expected to produce the greatest changes to rainfall characteristics and erosivity (Panagos et al., 2022; Zhao et al., 2021). If we can address this level of erosivity through various erosion control practices, we will be able to greatly reduce erosion/soil loss resulting from future climate changes. After applying quantile delta mapping (QDM) bias correction, these datasets were temporally downscaled to 15-min by Takhellambam et al. (2022). As recommended by McGehee and Srivastava (2018), 15-min rainfall datasets were used as a viable option to breakpoint rainfall for the estimation of rainfall erosivity (McGehee and Srivastava, 2018).

NA-CORDEX coverage included all of North America for the historical and future periods of 1970–1999 and 2030–2059, respectively. GCM simulations were forced with Coupled Model Intercomparison Project Phase 5 (CMIP5) under RCP8.5 scenario. Other scenarios (RCP2.5 and RCP4.5) were not downscaled to an hourly resolution. The original CMIP5 GCM outputs were downscaled via the NA-CORDEX to approximate temporal and spatial scales of 1-h and 50-km, respectively (Mearns et al., 2017; Scinocca et al., 2016). It should be noted that recent studies have reported that the CMIP Phase 6 (CMIP6) is an updated climate projection based on scenarios premises of CMIP5 and used socioeconomic pathways (van Vuuren and Riahi, 2011). The projections of CMIP5 are based on the radiative forcing values of four greenhouse gas concentration pathways of 2100 (Kamruzzaman et al., 2021; O'Neal et al., 2005). Chen et al. (2020) found that overall CMIP6 performed better than CMIP5 in simulating climate extremes of precipitation, especially with very heavy precipitation days (R20mm), maximum consecutive-5-day precipitation (RX5day), and consecutive dry days (CDD). Further, the uncertainty in CDD using the interquartile range (IQR) of CMIP6 was found to be smaller than CMIP5 (Li et al., 2021). Similarly, Li et al. (2021) found the uncertainty analysis for both annual total precipitation (PRCPTOT) and annual total precipitation with daily precipitation above 95th percentile (R95pTOT) of CMIP6 are found greater than that of CMIP5. In addition, Martel et al. (2022) found that CMIP6 has a narrow band of uncertainty with future climate projections, especially over North America. Overall, CMIP6 has better projection of future climate scenarios than CMIP5 (Chen et al., 2020). However, we are not considering CMIP6 in this study as CMIP6 has a coarser temporal resolution with the highest resolution of 1-h. We used recently developed 15-min rainfall which is downscaled from CMIP5 archive of NA-CORDEX as hourly rainfall datasets smoothed the rainfall intensities, resulting in an underestimation of erosivity (McGehee, 2016; McGehee and Srivastava, 2018; Takhellambam et al., 2022). However, future studies can use CMIP6 after the data has been appropriately downscaled.

2.2. Erosivity and erosivity density calculations

This study utilized WEPPCLIFF version 1.6 (McGehee et al., 2020) to perform erosivity calculations based on its Agricultural Research Service (ARS) energy equation option. This option returns results for all six of the major ARS erosivity and accompanying kinetic energy calculations (Table 2). Options include AH282, AH537, AH703, MM (McGregor and Mutchler, 1976), BF (Brown and Foster, 1987), and R2 (USDA-ARS, 2013, 2008). R2 is shorthand for RUSLE2. Therefore, this study computed six erosivity results for all GCM-RCM products and observed stations. Only the results based on the RUSLE2 energy equation were reported in this manuscript since that is the most popular rainfall erosivity in the United States currently. Although the RUSLE2 energy equation was used to calculate erosivity (Eqs. (1)–(3)), not all RUSLE2 rules were applied due to concerns raised in McGehee et al. (2022, 2021) over the omission of some storms, where 'storm' is defined as a continuous sequence of precipitation, separated by 6 h or more with <1.27 mm of precipitation (Wischmeier and Smith, 1978). More specifically, small storms were not omitted and storms of return period >50-years were not omitted from the analysis. The prior references provide strong cases for decisions to retain all storms in various erosivity analyses if one requires more information. Similar to McGehee and Srivastava (2018), all precipitation was assumed to be rainfall in both observed and modeled climate data. Snowfall amounts in particular should not be used to calculate erosivity, and snowfall should be removed from analyses of rainfall erosivity elsewhere in the United States (McGehee et al., 2022). However, snowfall is uncommon in the vast majority of the Southeast US, and it is projected to become rarer in the future. Therefore, this assumption would have negligible effects on results of this study.

$$\mathrm{R}\left(\mathrm{MJ\ mm\ ha^{-1}h^{-1}yr^{-1}}\right) = \frac{1}{\mathrm{n}}\sum_{\mathrm{j}=1}^{\mathrm{n}}\left[\sum_{k=1}^{m}(E_s)_k\right] \quad (1)$$

where R is rainfall erosivity also known as R-factor (MJ mm ha^{-1}h^{-1}yr^{-1}); n is number of years; m is number of storms in each year; j and k are index of number of years and storms in each year, respectively, and E_s is storm erosivity (Eq. (2)).

$$\mathrm{E_s}\left(\mathrm{MJ\ mm\ ha^{-1}h^{-1}}\right) = \left(\sum_{\mathrm{t}=1}^{\mathrm{p}}\mathrm{e.P}\right).\mathrm{I_{30}} \quad (2)$$

Table 2
The most used six rainfall kinetic energy equations. Units are in kinetic energy per unit volume of rain in MJ mm^{-1} ha^{-1}, and i is the rainfall intensity in mmh^{-1}.

Sl. No	Name of rainfall Kinetic energy	Energy equation
1	Agricultural Handbook No. 282 (AH282)	$e_{AH282} = 0.119 + 0.0873\ log_{10}(i)$
2	Agricultural Handbook No. 537 (AH537)*	$e_{AH537} = 0.119 + 0.0873 log_{10}(i)$
3	Agricultural Handbook No. 703 (AH703)*	$e_{AH703} = 0.119 + 0.0873\ log_{10}(i)$
4	McGregor and Mutchler (MM)	$e_{MM} = 0.273 + 0.2168e^{(-0.048i)} - 0.4126e^{(-0.072i)}$
5	Brown and Foster (BF)	$e_{BF} = 0.29(1 - 0.72\ e^{(-0.05i)})$
6	Revised Universal Soil Loss Equation version 2 (RUSLE2 or R2)	$e_{R2} = 0.29 * (1 - 0.72\ e^{(-0.082i)})$

*Both AH537 and AH703 have kinetic energy limits imposed at 76 mm h^{-1} and AH537 has a 30-min maximum intensity limit imposed at 64 mm h^{-1}.

where e is the rainfall kinetic energy per unit depth (Eq. (3)); t is single time interval; p is number of time segments in the event; P is rainfall depth (mm); and I_{30} is maximum 30-min rainfall intensity.

$$e\left(MJ\ ha^{-1}mm^{-1}\right) = 0.119 + 0.0873 * \log_{10}(I) \quad (3)$$

where, I is rainfall intensity (mm h^{-1}).

Erosivity density (ED) calculations were not supported by WEPPCLIFF at the time this study was conducted. To obtain erosivity density values, the storm data export option in WEPPCLIFF was used, and erosivity densities were calculated from the resulting storm R and precipitation values. The same procedure used by Kinnell (2010) was used for these calculations. as provided in Eq. (4).

$$ED_j\ \left(MJ\ ha^{-1}h^{-1}\right) = \frac{R_j}{P_j} \quad (4)$$

where, R and P are annual rainfall erosivity and precipitation depth (mm), respectively, for j^{th} year.

Erosivity density provides both erosivity pattern as well as precipitation type for erosive events. For instance, high erosivity density resulted from a high intensity rainfall event of short duration (Zhu et al., 2021). ED are typically favored in cases with shorter station record lengths, excessive data gaps, no locally measured precipitation characteristics, or more generally when the variability of erosivity presents a challenge. On the other hand, the standard approach, in which all precipitation data is used for erosivity calculation and no extrapolation relationship is necessary, may offer more insight into more subtle patterns of erosivity. This is the same approach used in the original Wischmeier and Smith (1958) discovery and underlying theory, which were established using breakpoint precipitation data. Unfortunately, some inconsistent application of that theory and other erosivity practices have resulted in published discrepancies in peer-reviewed literature (McGehee et al., 2021). This presents a challenge for studies of projected erosivity, since in addition to modeling and climate change uncertainty, there appear to be uncertainties in how to apply the original erosivity theory to various precipitation data types and their impacts on precipitation characteristics, especially intensity. Hopefully, with time, both of these sources of uncertainty will be reduced or eliminated. Until then, it is important for readers to take note of the methods utilized to arrive at various erosivity results.

2.3. Extreme value analysis of rainfall and erosivity

We used the annual maxima series (AMS) method for comparing the extreme rainfall events between projected future and historical climate simulations. A generalized extreme value (GEV) probability distribution was selected as suggested by Op de Hipt et al. (2018) and Mirhosseini et al. (2013) to fit the rainfall distribution of annual daily maximum values. This distribution combines three parameter distributions i.e., Gumbel, Frechet, and Weibull which is based on the extreme value theory (Coles et al., 2001; Op de Hipt et al., 2018; Zhao et al., 2021). The fitted distribution was then used to obtain the annual daily maximum rainfall for the following return periods: 2-, 5-, 10-, 25-, and 50-years. Additionally, the effects of extreme events on rainfall erosivity were analyzed using these annual maximum storm frequencies.

Moreover, the null hypothesis (H0: historical and future projected parameters come from the same distribution) was tested using either paired sample *t*-test, Wilcoxon sign test, or both (Op de Hipt et al., 2018). The test method was selected based on the characteristics of datasets according to the following rules. Both the paired sample t-test and the Wilcoxon sign test were used when the assumptions of normality were satisfied. Only the Wilcoxon sign test was used when the datasets were not normally distributed. The Shapiro-Wilk Test was used to determine normality for the selection of other test methods.

3. Results and discussions

In this section, we report results obtained for observed (1970–2013) station data and five RCM-GCM products with both historical (1970–1999) and future (2030–2059) time periods for precipitation, rainfall erosivity, and erosivity density. The similarity of observed and historical climate results is discussed first. Then, results based on future projections are compared to historical simulations.

3.1. Precipitation

The observed average annual precipitation across all stations ranged from 835 to 1689 mm yr^{-1} with a mean of 1231 mm (Fig. 1). The spatial distribution of observed precipitation shows that greater rainfalls are received at Gulf-Atlantic coast and the Appalachian Mountain. Moreover, bias-corrected historical model simulations (1970–1999) of average annual precipitation were generally greater than observed precipitation patterns (Fig. 2). Almost all statistical measures of the ensemble-average historical simulations were >20 % different from observed measures. The values for standard deviation, coefficient of variation, and maximum average annual precipitation were most different from observed measures (Table 3).

The average annual precipitation for projected future simulations was significantly greater as compared to historical simulations (Fig. 2). All the models reject the null hypothesis of equal average annual precipitation between the historical and future period (*p*-value <0.05) favoring the alternate hypothesis at 5 % significance level using the Wilcoxon Rank test. Future (2030–2059) average annual precipitation ranged from 1641 to 1993 mm yr^{-1}. The minimum and maximum average annual precipitation were 800 and 4015 mm yr^{-1}, respectively. Outliers (as determined by 1.5 times the interquartile ranges (IQR) in both upper and lower quartile) in average annual precipitation were present in all climate models which showed a relatively high spatial variability of average annual precipitation for this region which tends to be less varied than in the western US. Among the five models in this study, HADGEM, MPIREG and MPIWRF resulted in greater mean, median, and variability (IQR and outliers) of average annual precipitation. The ensemble mean of projected future precipitation showed an increase in average annual precipitation of 14 % as compared to the historical model ensemble mean of 1638 mm yr^{-1}. This was as little as 7 % and as great as 25 % when considering individual stations in the Southeast US, so according to this analysis there is a substantial amount of spatial variability in projected changes to precipitation in this region.

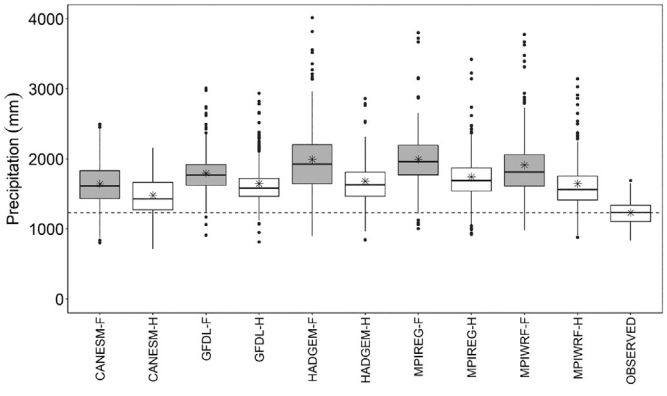

Fig. 2. Boxplots for observed, historical and future average annual precipitation over the Southeast US. Each point represents an average annual precipitation for a single station. 'H' and 'F' at the end of model's name indicate 'historical' and 'future' model simulations, respectively. Asterisk (*) indicates the average value. Dotted line represents the mean value of observed average annual precipitation of 187 stations from 1970 to 2013.

Table 3
Bias-corrected average annual precipitation statistics for 187 locations in the southeastern US for observed DSI-3260 gauge data (1970–2013) and five RCM-GCM simulations of historical (1970–1999) and future (2030–2059) periods from NA-CORDEX. Observed differences were calculated using the observed data mean as the baseline. Simulated differences were calculated using the respective historical model simulation mean as the baseline.

Statistic	OBSERVED	CANESM-H	GFDL-H	HADGEM-H	MPIREG-H	MPIWRF-H	CANESM-F	GFDL-F	HADGEM-F	MPIREG-F	MPIWRF-F
Min.	835	711	811	839	919	878	800	909	895	1001	981
Med.	1233	1427	1583	1627	1688	1563	1611	1768	1925	1957	1812
Max.	1689	2156	2933	2859	3419	3143	2492	3007	4015	3802	3775
Std.Dev.	160	300	340	347	379	382	332	320	530	403	487
COV	0.13	0.20	0.21	0.21	0.22	0.23	0.20	0.18	0.27	0.20	0.25
Mean	1231	1478	1645	1681	1742	1646	1641	1795	1993	1992	1912
Obs.Abs.Diff.	0	247	414	450	511	414	410	564	762	761	681
Obs.Rel.Diff.	0 %	20 %	34 %	37 %	42 %	34 %	33 %	46 %	62 %	62 %	55 %
Sim.Abs.Diff.							164	149	312	250	266
Sim.Rel.Diff.							11 %	9 %	19 %	14 %	16 %

3.2. Rainfall erosivity

The annual rainfall erosivity was calculated for 187 stations using the RUSLE2 energy equation without omitting any storms based on recommendations from McGehee and Srivastava (2018) and McGehee et al. (2022, 2021) over the Southeast United States (Table 4). These erosivities obtained using gauge data were further used to develop the spatial variation using kriging interpolation for ensemble model for the Southeast United States (Fig. 3). The erosivity patterns were found consistent from prior maps published in the agricultural handbooks, and spatial patterns were consistent in maps for observed, historical, and future periods. As expected, erosivity in the Gulf and Atlantic coastal areas and Appalachian

Table 4
Average annual erosivity statistics for 187 locations in the southeastern US for observed DSI-3260 gauge data (1970–2013) and five RCM-GCM simulations of historical (1970–1999) and future (2030–2059) periods from NA-CORDEX using R2 approach (without data limitations). Observed differences were calculated using the observed data mean as the baseline. Simulated differences were calculated using the respective historical model simulation mean as the baseline.

Statistic	OBSERVED	CANESM-H	GFDL-H	HADGEM-H	MPIREG-H	MPIWRF-H	CANESM-F	GFDL-F	HADGEM-F	MPIREG-F	MPIWRF-F
Min.	1273	1501	1686	1742	1807	1760	2186	2112	3174	2277	2419
Med.	4043	5806	6641	6975	6814	6272	9116	8546	10,950	10,995	8969
Max.	10,587	15,699	22,439	19,918	27,286	23,058	31,408	35,333	38,125	35,753	41,256
Std.Dev.	1860	2748	3549	3566	4165	3953	4742	4283	6596	5788	6412
COV	0.41	0.42	0.45	0.44	0.51	0.51	0.48	0.44	0.51	0.47	0.57
Mean	4546	6527	7821	8075	8130	7773	9971	9655	12,985	12,366	11,206
Obs.Abs.Diff.	0	1981	3275	3528	3583	3226	5425	5108	8438	7820	6660
Obs.Rel.Diff.	0 %	44 %	72 %	78 %	79 %	71 %	119 %	112 %	186 %	172 %	146 %
Sim.Abs.Diff.							3444	1834	4910	4237	3433
Sim.Rel.Diff.							53 %	23 %	61 %	52 %	44 %

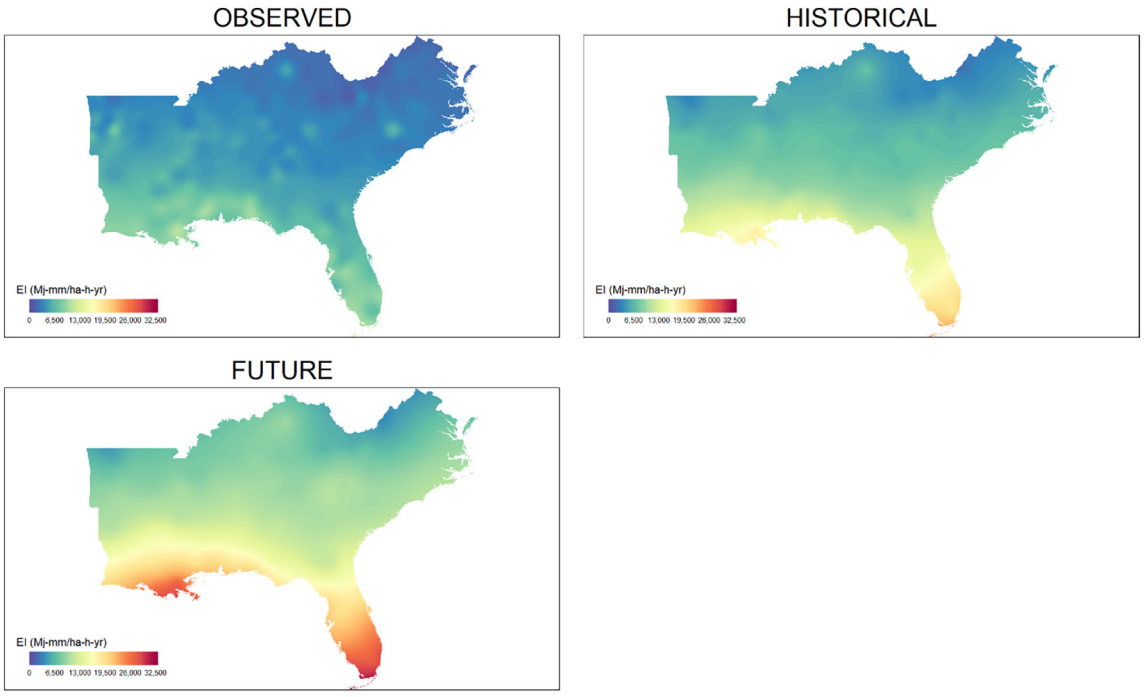

Fig. 3. Observed (1970–2013) and ensemble mean annual rainfall erosivity (R-factor) over the Southeast United States using the RUSLE2 energy equation (without data limitations) via WEPPCLIFF v1.6 for the historical (1970–1999) and projected future (2030–59) periods.

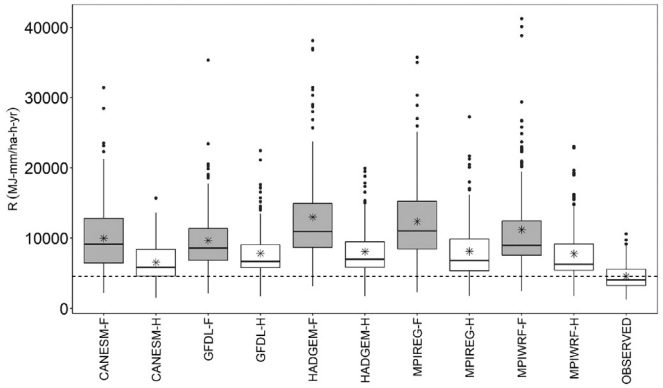

Fig. 4. Boxplots for observed, historical and future average annual erosivity over the Southeast United States. Asterisk (*) indicates the average value. Dotted line represents the mean value of observed average annual rainfall erosivity of 187 stations from 1970 to 2013.

Mountain regions was greater than in other inland regions. This shows a similar trend with the patterns of greater precipitation found in these regions (Fig. 1). The observed annual R-factor of 187 stations from 1970 to 2013 was obtained ranging from 1273 to 10,587 MJ mm $ha^{-1}h^{-1}yr^{-1}$ (Table 4 and Fig. 4). In addition, the observed average annual R-factor has value of 4546 MJ mm $ha^{-1}h^{-1}yr^{-1}$. As anticipated, the maximum annual R-factor was found in the eastern Louisiana which is in close proximity to the Gulf of Mexico. Whereas the minimum annual R-factor was found in the north boundary of Virginia, where the precipitation decreases further inland from the Gulf-Atlantic coast. These observed erosivity results are consistent with previous erosivity mapping studies (McGehee and Srivastava, 2018; McGehee et al., 2022) and were consistent with the erosivity benchmarking study by McGregor et al. (1995).

Although, the minimum and maximum annual R-factor under five historical models from 1970 to 1999 were found in CANESM and MPIREG with 1501 and 27,286 MJ mm $ha^{-1}h^{-1}yr^{-1}$, respectively. This range was a much greater than observed, and was as much as 158 % greater for some stations. The observed data was gap-filled, but they were not corrected for gauge undermeasurement bias. This bias can range from 0 % to 10 % for gauges installed above ground level in various wind conditions (Rodda, 1967; Rodda and Dixon, 2012). However, this potential downward bias is small compared to the differences obtained in this analysis. Similar to that of precipitation, reasons for these differences in erosivity, are discussed later in detail.

In the case of future period of 2030–2059, average annual R-factor in five models ranged from 9655 (GFDL) to 12,985 (HADGEM) MJ mm $ha^{-1}h^{-1}yr^{-1}$. In addition, the minimum and maximum annual R-factor were found under GFDL and MPIWRF with 2112 and 41,256 MJ mm $ha^{-1}h^{-1}yr^{-1}$, respectively. These results show that the average annual future projected rainfall erosivity are significantly greater than the historical period (1970–1999) of CANESM, HADGEM, GFDL, MPIREG, and MPIWRF models (Table 4). Among the various climate models, HADGEM MPIREG, and MPIWRF resulted in the greatest projected average annual rainfall erosivities consistent with each of these models projecting the greatest average annual precipitations as well (Table 3).

Given that these simulated climate data were downscaled as part of standard NA-CORDEX procedures and further downscaled by Takhellambam et al. (2022), we investigated whether these erosivities were being driven by a few high-intensity events. The same erosivity analysis was performed excluding events with intensities >401 mm hr^{-1} which may be considered as outliers (Lewis et al., 2021). Unfortunately, the resulting erosivities were not significantly different from the previous datasets, which reduced average annual values by <1 %. Provided the insignificant impact of these relatively extreme events, we retained all events in our various analyses. Therefore, the main reason for large differences and variation of erosivity among the different models was due to the large storm depths which may have been introduced by bias correction or downscaling.

To quantify the projected change in average annual erosivity, we computed the relative change in erosivity with reference to the respective historical model as the baseline (Table 4). The results show that the projected relative change in the average annual R-factor ranged from 23 % to 61 % or an ensemble average of 47 %. Results were consistent with previous studies which also showed a similar trend in increasing projected rainfall erosivity for the region (Biasutti and Seager, 2015; Hoomehr et al., 2016; Nearing, 2001). This analysis indicated that parts of the Southeast US with the greatest precipitation may see the greatest increase in R-factor (Fig. 3). These areas include the most southern part of Florida, the Appalachian region, and the Gulf-Atlantic coast. However, it is unclear how much of these potential increases were influenced by suboptimal bias correction or downscaling and is discussed in detail later.

The effect of extreme rainfall events on R-factor was investigated using the annual maximum storm events from historical and future scenarios. Under all of the models, increase in the erosivity due to maximum storm events ranged from 30 % to 87 % (Fig. 5). We further found that majority of the stations have significantly increased erosivity in the future projected scenarios as compared to the historical scenario. We found range of annual maximum erosivity ranges from −10 % to 393 %. One of the main reasons is due to the significant increase in the extreme rainfall intensity.

3.3. Erosivity density

Erosivity density (ED) was calculated for each station with an observed average annual value of 3.6 MJ $ha^{-1}h^{-1}yr^{-1}$ (Table 5 and Fig. 6). The historical and future ensemble mean of annual ED was 4.49 and 5.76 MJ $ha^{-1}h^{-1}yr^{-1}$, respectively (Table 5). In relative terms, ED based on historical simulations was 25 % greater than observed ED, but this was smaller than differences for both precipitation and erosivity which were 33 % and 69 %, respectively. The results from both paired sample test and Wilcoxon rank test found rejecting the null hypothesis of equal erosivity density between the historical and future scenarios at a 5 % significance level with p-value <0.05. Therefore, projected ED was 29 % significantly greater than historically simulated ED, which means that simulated changes due to climate were greater than differences between historical simulations and observed data.

Similar to precipitation and erosivity analyses presented earlier, ED results could have been impacted by bias correction of downscaling methods. It is possible that impacts on the wettest stations' precipitation and resulting erosivity calculations could result in biased ED calculations due to the nonlinear behavior of erosivity. Therefore, although ED accounts for differences in precipitation amount, it would not account for a potential

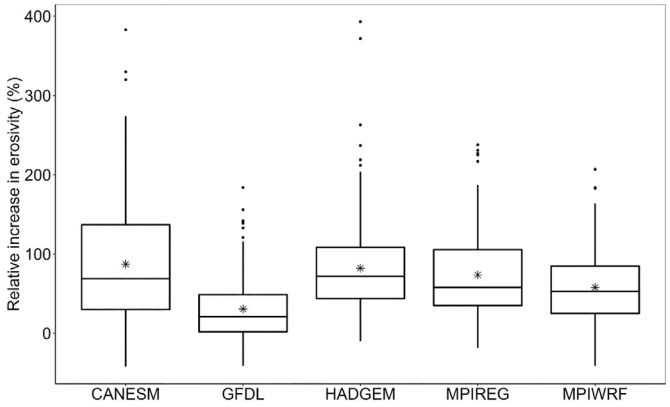

Fig. 5. The relative increase in the annual maximum erosivity due to the annual maximum storm event using five climate models under the RCP8.5 scenario. Asterisk symbols denote the mean value.

Table 5
Average annual erosivity density statistics for 187 locations in the southeastern US for observed DSI-3260 gauge data (1970–2013) and five RCM-GCM simulations of historical (1970–1999) and future (2030–2059) periods from NA-CORDEX. Observed differences were calculated using the observed data mean as the baseline. Simulated differences were calculated using the respective historical model simulation mean as the baseline.

Statistic	OBSERVED	CANESM-H	GFDL-H	HADGEM-H	MPIREG-H	MPIWRF-H	CANESM-F	GFDL-F	HADGEM-F	MPIREG-F	MPIWRF-F
Min.	1.36	1.92	2.07	2.06	1.92	2.00	2.40	2.31	3.03	2.15	2.36
Med.	3.35	4.14	4.43	4.46	4.15	4.26	5.58	4.95	5.97	5.66	5.19
Max.	6.59	7.38	8.06	7.91	7.98	8.32	13.73	11.75	10.68	11.04	12.16
Std.Dev.	1.14	0.98	1.15	1.14	1.34	1.22	1.83	1.41	1.51	1.76	1.63
COV	0.32	0.23	0.25	0.25	0.30	0.27	0.31	0.27	0.24	0.29	0.29
Mean	3.60	4.25	4.58	4.63	4.45	4.52	5.83	5.21	6.22	5.98	5.55
Obs.Abs.Diff.	0.00	0.64	0.98	1.03	0.85	0.91	2.23	1.61	2.62	2.38	1.95
Obs.Rel.Diff.	0 %	18 %	27 %	29 %	24 %	25 %	62 %	45 %	73 %	66 %	54 %
Sim.Abs.Diff.							1.58	0.63	1.59	1.53	1.04
Sim.Rel.Diff.							37 %	14 %	34 %	34 %	23 %

nonlinear bias in wetter parts of the Southeast. These issues and the actions taken to account for them are discussed below.

3.4. Comparison of rainfall erosivity map among different studies

The comparison of estimated future erosivity with previous studies is challenging. This is due to the different erosivity estimation methods and frameworks employed by various studies. In addition, the different time scales and uncertainty associated with different GCMs and downscaling methods further contributed to the differences in erosivity estimations (Panagos et al., 2022). The climate models are associated with different variations depending upon the type of model, e.g., initial and boundary conditions of the rainfall generation mechanism (Mirhosseini et al., 2013). However, we were able to compare the findings of a previous study by Panagos et al. (2022) which projected erosivity for 20 years (2041–2060) using 30-min rainfall, estimated with HADGEM and MPIREG models under RCP8.5 scenario over the Southeast United States. We estimated the annual R-factor using 30-min (aggregated 15-min to 30-min rainfall) rainfall data with HADGEM and MPIREG model under the RCP8.5 scenario for the 20 years (2040–2059) to compare with Panagos et al. (2022).

Using the HADGEM model (Fig. 7a), Panagos et al. (2022) reported that the annual R-factor from 2041 to 2060 varies from 1501 to 11,249 MJ mm $ha^{-1}h^{-1}yr^{-1}$ with an average value of 7137 MJ mm $ha^{-1}h^{-1}yr^{-1}$. In our study, the average annual R-factor showed 11,190 MJ mm $ha^{-1}h^{-1}yr^{-1}$ which is found greater by 56 %. The change in annual R-factor based on our approach as compared to the Panagos et al. (20022) ranged from −67 % to 1167 % (Fig. 7b). Similarly, the MPIREG model showed a consistent result with relatively greater annual R-factor in the Gulf-Atlantic coastal regions as compared to the Panagos et al. (2022) (Fig. 7c and d). Under the MPIREG model, the reported range of annual R-factor by Panagos et al. (2022) was 1240 to 10,851 MJ mm $ha^{-1}h^{-1}yr^{-1}$ with an average value of 6705 MJ mm $ha^{-1}h^{-1}yr^{-1}$ (Fig. 7b). Our study showed an average annual R-factor of 11,917 MJ mm $ha^{-1}h^{-1}yr^{-1}$. In addition, the relative change in annual R-factor under MPIREG model in our study shows in the range of −50 % to 1234 % as compared to that of Panagos et al. (2022).

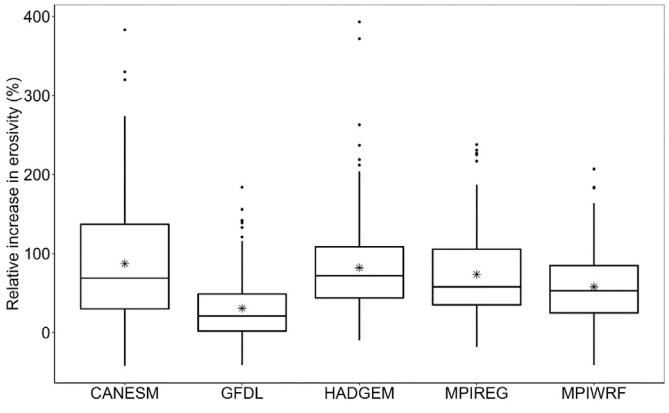

Fig. 6. Boxplots for observed, historical and future average annual erosivity density over the Southeast United States. Asterisk (*) indicates the mean value. Dotted line represents the mean value of observed average annual rainfall density of 187 stations from 1970 to 2013.

The negative and positive values (Fig. 7b and d) indicate a lower and greater values of annual R-factor in our study with reference to Panagos et al. (2022), respectively. In both models, the lowest and greatest change in annual R-factor was found in the northern and southern parts of the region, especially in the Gulf-Atlantic coastal region. However, the majority of the area showed relatively smaller change (up to 100 %) with 0 % indicating no change in the annual R-factor (light green color in Fig. 7b and d).

4. Discussion

4.1. Future erosivity using high-temporal resolution rainfall datasets

The accurate estimation of rainfall erosivity requires high temporal resolution of rainfall datasets (Kim et al., 2020; McGehee and Srivastava, 2018; McGehee et al., 2022; Panagos et al., 2017). McGehee and Srivastava (2018) and McGregor et al. (1995) further encouraged to use "breakpoint" rainfall datasets for the estimation of erosivity. Therefore, our study used recently developed 15-min rainfall data from CMIP5 archive for future (2030–2059) erosivity estimation over the Southeast United States as a viable option to breakpoint datasets (McGehee and Srivastava, 2018; Takhellambam et al., 2022). The differences in observed and historical simulated rainfall data could have arisen from slightly different time periods, model or downscaling limitations (e.g., course resolution, incomplete model science, model stochasticity), bias correction, observed data limitations (e.g., gaps or undermeasurement bias), or a combination of these. The impacts of these differences on this study are discussed later at Section 4.2 in detail. Although, the significant different between the historical and future rainfall datasets confirmed that by 2059, the region is expected to receive a significant number of intense rainfalls compared to the historical period of 1970–1999. This necessitates updating the estimation of future rainfall erosivity with high temporal resolution rainfall datasets (McGehee and Srivastava, 2018; Takhellambam et al., 2022).

Previous studies used aggregated rainfall due to the unavailability of rainfall datasets (Biasutti and Seager, 2015; Hoomehr et al., 2016; Nearing, 2001; Panagos et al., 2022). These rainfall datasets of lower temporal resolution lose the information of true rainfall characteristics. Takhellambam et al. (2022) showed that the downscaled 15-min rainfall datasets exhibit intensities that are greater than the 1-hourly scale but lower intensities than the observed 15-min rainfall. The rainfall intensity using aggregated rainfall datasets has often been underpredicted as compared to the 15-min datasets due to the smoothening of the intensities and eventually lower erosivity (McGehee and Srivastava, 2018; McGehee et al., 2022; Op de Hipt et al., 2018). For example, the annual erosivity from Kim et al. (2020) was found to be under-predicted as compared to our study. This was expected because Kim et al. (2020) used 1-h grided

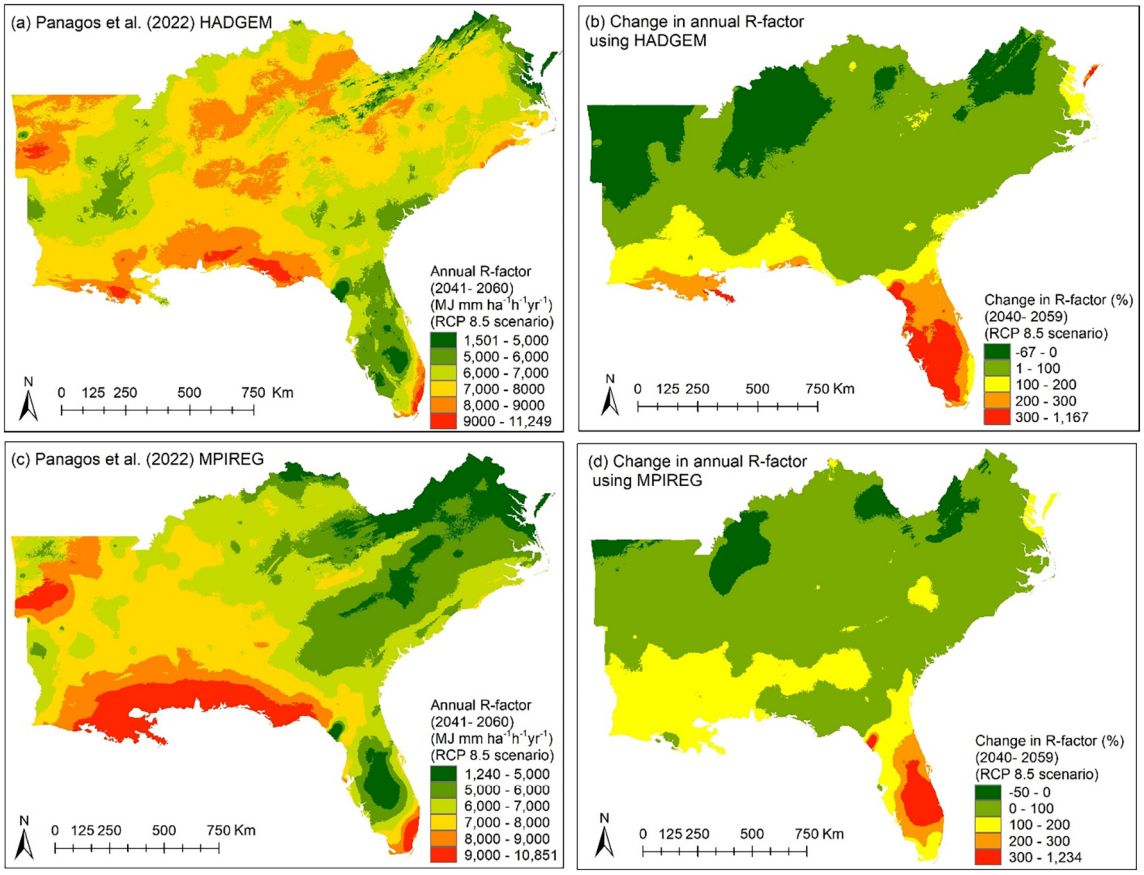

Fig. 7. (a) and (c) Reported annual R-factor of Panagos et al. (2022) for HADGEM and MPIREG model under RCP8.5 scenario for 20 years (2041–2060) using Gaussian Process Regression. (b) and (d) relative change in annual R-factor (in percentage) in our study as compared to Panagos et al. (2022) under same HADGEM and MPIREG model for 20 years (2040–2059). Negative and positive value indicates the lower and greater annual R-factor in our study with reference to the Panagos et al. (2022), respectively.

rainfall to estimate erosivity. Kim et al. (2020) reported a maximum value of 6000 MJ mm $ha^{-1}h^{-1}yr^{-1}$ with a mean value of <2500 MJ mm $ha^{-1}h^{-1}yr^{-1}$. Whereas, our study showed greater erosivity as compared to Kim et al. (2020) because we use 15-min rainfall datasets that give improved estimates of intensities as compared to the hourly rainfall. Hollinger et al. (2002), McGehee and Srivastava (2018), and USDA-ARS (2008) have suggested that we further increase erosivity obtained from the 15-min rainfall datasets by 4 % to compensate for the dampening in intensity with the use of fixed-interval data (e.g., 15-min) as compared to breakpoint data.

The future erosivity showed a large variation among the stations which can be seen from the boxplot (Fig. 4) and large standard deviation values in Table 4. These variations are owed to the large variation of rainfall due to the extreme rainfall intensities (Fig. 2). Furthermore, this can be confirmed by the higher ED (>3 MJ ha^{-1} h^{-1}) indicating that the precipitation has higher intensities for short-duration rainfall events (Chen et al., 2022; Panagos et al., 2015).

Each RCM-GCM shows different amounts of rainfall due to the different mechanisms of rainfall generation. Therefore, the ensemble model of five RCM-GCMs allows a representative estimation of future rainfall erosivity under the RCP8.5 scenario. This prevents the result from being influenced by a single model (Panagos et al., 2022). Moreover, kriging interpolation has enabled us to evaluate the spatial variation of erosivity using the rain-gauge approach (Kim et al., 2020; McGehee and Srivastava, 2018). The greater amount of annual R-factor in the Gulf-Atlantic coast owes to the greater precipitation because of warm air rising through sea breeze circulation. Precipitation decreases further inland and with increasing elevation and reduced moisture holding capacity of cooler air (Ingram et al., 2013). Greater precipitation was observed in the Appalachian Mountains due to orographic effects leading to greater erosivity in the region (Ingram et al., 2013).

A comparison of the findings of this study with those of Panagos et al. (2022) shows relatively similar trends of erosivity in majority parts of the region. However, there is a greater estimation of erosivity in this study, especially in the Gulf-Atlantic coastal region and southern Florida. We anticipated a greater amount of erosivity as the region receives a greater amount of rainfall owing to the convective precipitation and tropical cyclones (Ingram et al., 2013; Knight and Davis, 2007). Panagos et al. (2022) used two stations in southern Florida to estimate erosivity, whereas our study used denser rain-gauge data of 16 (Fig. 1), which could have resulted in erosivity differences. In addition, the greater amount of annual erosivity in our study, especially in the Gulf-Coastal area could be due to various reasons. For instance, Panagos et al. (2022) estimated the annual R-factor using a regression model, whereas our study estimated the same based on rainfall storm events. The true rainfall characteristics, such as intensity are lost while using the statistical relationships for the estimation of erosivity (Flanagan et al., 2020; Hollinger et al., 2002; McGehee et al., 2022). Our study also used in-situ rainfall datasets which are superior to the grid-based datasets of Panagos et al. (2022), especially with high-intensity rainfall events (Kim et al., 2020). In addition, differences in amounts of annual erosivity among the models is also caused due to different mechanisms of rainfall generation employed within each model (Mirhosseini et al., 2013).

Regardless of the models and erosivity application methods used, the region is expected to have significantly higher future annual erosivity than in the historical period. Furthermore, the region's elevated rainfall erosivity is

caused by increased rainfall intensity (Swain and Hayhoe, 2015). However, there are some uncertainties associated with our study, which are discussed in detail below.

4.2. Bias correction and downscaling implications

Bias correction (BC) and downscaling (DS) were both potential sources of differences between observed and historical model simulation results. BC led to increasing average annual precipitation and intensities. While downscaling led to a decrease in moderate rainfall intensities. However, the downscaled results showed higher intensities than the hourly although lower than the observed 15-min precipitation (Takhellambam et al., 2022). In this study, we used relatively high-temporal resolution, 15-min historical, and projected precipitation datasets generated from hourly NA-CORDEX products by Takhellambam et al. (2022). That study used quantile delta mapping (QDM) and a modified stochastic disaggregation method for bias correction and further downscaling of NA-CORDEX climate products, respectively. There were substantial differences between historical simulations and observations of precipitation, erosivity, and erosivity density (Table 3-5 and Figs. 2, 4, and 6). In comparison to the observed annual R-factor, the bias-corrected and non-bias-corrected annual R-factors had overestimated and underestimated values by 137 % and − 63 %, respectively. It is currently unclear if there are other BC and DS methods that would result in better agreement with observed data especially with hourly scale since, to our knowledge, this has not been studied and published in the peer-reviewed literature for erosivity-based analyses.

The goal of this study was to quantify projected mid-century changes in erosivity for the Southeast US and to do this using an erosivity approach of RUSLE2 with recommendations of McGehee and Srivastava (2018) and McGehee et al. (2022,2020) rather than an oversimplified erosivity extrapolation or aggregation method that assumes a relationship to historical precipitation characteristics. This approach to analyzing projected future erosivity is more rigorous than others, but there are potential sources of uncertainty in the estimated future rainfall erosivity, especially with the BC and DS.

To assess the performance of bias correction, Takhellambam et al. (2022) evaluated average annual precipitation, wet-hour frequencies, and precipitation intensities. Although the intensities and wet-hour frequencies were improved, the average annual precipitation was largely over-corrected or overpredicted. As expected, the uncorrected historical model simulations of average annual precipitation were greater than observed due to potential under-measurement biases in the observed data generated by adhesion, evaporation, wind drift, and splashing (Table 6) (Fischer et al., 2018) and model biases in the simulated data. However, bias correction of the simulated results worsened average annual precipitation differences which increased by 3.5 % to 19.2 % over what was already consistently greater than observed. This, along with the increased presence of more extreme event depths and characteristics, was largely responsible for the greater mean and maximum average annual erosivity values obtained in this study. The results showed that the extreme event depths significantly increased as the null hypothesis was rejected at the 5 % significant level. The mean relative increase (in percentage) of annual daily maximum rainfall with reference to the historical model ranges from 8 % to 46 % (Table 7).

Table 6
Percentage change in average annual precipitation after bias correction of climate models used in Takhellambam et al. (2022). Here, Raw and BC denotes the ratio of average annual precipitation of historical model and observed precipitation before and after bias correction.

Model	Raw	BC	Change (%)
CANESM	1.09	1.26	15.56
HADGEM	1.39	1.44	3.50
GFDL	1.32	1.41	6.82
MPIREG	1.34	1.50	11.74
MPIWRF	1.19	1.42	19.23

Table 7
Mean relative change (%) in future projected annual daily maximum rainfall as compared to the historical model with return period of 2-, 5-, 10-, 25-, and 50-years.

Model	2-years	5-years	10-years	25-years	50-years
CANESM	17	32	38	43	45
GFDL	8	12	13	15	15
HADGEM	22	35	39	44	46
MPIREG	21	27	29	31	32
MPIWRF	19	24	26	28	30

While the additional downscaling method used by Takhellambam et al. (2022) was another potential source of uncertainty in this analysis, it was unlikely that this method resulted in upward biases in this study's analyses. We base this assessment on the results presented by Takhellambam et al. (2022) showing that there was a substantial downward bias in 15-min intensities obtained from their DS method as compared to those from observed data. More specifically, the intensities were greater than those of simulated hourly data but less than those of observed 15-min data. According to Flanagan et al. (2020), this would result in a substantial underestimation (at least 9 %) of erosivities that would be obtained from breakpoint precipitation gauges at the same location. We found the temporal downscaling using a modified stochastic approach has led to the underestimation of erosivity with an average value of 17 %. This is because the downscaled rainfall characteristics do not adequately represent the observed rainfall characteristics (Takhellambam et al., 2022). Overall, these findings highlight the uncertainties of using climate models for high-resolution applications and their limitations in representing rainfall characteristics. In light of potential bias correction limitations, it may be of interest to evaluate downscaled, uncorrected climate simulations for analyses involving erosivity. The newest generation of climate model simulations, which are being conducted at increasingly finer spatial and temporal resolutions, may meaningfully reduce uncertainties from BC and DS methods in subsequent analyses.

5. Conclusions

The most significant finding of this study is that precipitation, erosivity, and erosivity density in the Southeast US are projected to increase by 14 %, 47 %, and 29 %, respectively, for 2030–2059 over the historical baseline (1970–1999). These results were obtained using an ensemble of five different climate models in NA-CORDEX which is an archive of CMIP5 under the RCP 8.5 scenario. CMIP6 has better future climate projection with a narrower uncertainty band as compared to CMIP5. However, the temporal resolution of CMIP6 is 1 h, which makes it unsuitable for the estimation of erosivity until it is downscaled to 15-min resolution. Therefore, in this study, we have used a recent 15-min precipitation dataset that was downscaled using the CMIP5 dataset.

We used WEPPCLIFF version 1.6 and the RUSLE2 energy equation without data limitations for the estimation of rainfall erosivity and erosivity density. The future ensemble model showed an average annual R-factor of $11{,}237 \pm 1299$ MJ mm $ha^{-1}h^{-1}yr^{-1}$. The southern part of Florida, the Appalachian region, and the coastal region of the Gulf of Mexico were areas in the Southeast predicted to experience the greatest absolute increase in erosivity while areas with lower baseline erosivities were generally predicted to see the largest relative changes.

Erosivity and erosivity density outcomes in this study were determined as opposed to aggregation or extrapolation methods which have become more common of late. This was an important decision of this study which can potentially reduce uncertainties associated with assuming historical precipitation characteristics for future periods. However, as discussed earlier, this decision also may have resulted in greater exposure to bias correction and downscaling method limitations. For instance, downscaling alone was determined to suppress erosivity estimates by 17 % in an analysis using this study's observed data. The bias correction of rainfall overestimated the annual R-factor with an average of 137 %, whereas non-bias corrected data underestimated the R-factor with an average of 62 % when compared to the

observed annual R-factor. Average annual precipitation, erosivity, and erosivity densities obtained from bias-corrected and downscaled historical model simulations were consistently greater than observed values. Some degree of this should be expected on account of under-measurement biases associated with the observed data; however, the differences obtained in this study were much greater than can be attributed to that dynamic alone. Therefore, alternative bias correction and downscaling methods should be evaluated for potential use with subsequent erosivity analyses which may result in better agreement between historical simulations and observed metrics.

Results of a similar study with different bias correction and/or downscaling methods could result in very different outcomes, especially since erosivity increases with total rainfall depth, rainfall intensity, or frequency of wet days. In addition, future research needs to be conducted with different biases and downscaling methods. Despite these uncertainties, this study affirms that projected climate change is likely to increase erosion in the Southeast US and that this increase will not be driven by changes in precipitation amounts alone but also due to changes in intensity and energy.

CRediT authorship contribution statement

Bijoychandra S. Takhellambam: Conceptualization, Methodology, Formal analysis, Data curation, Writing - original draft & review, Visualization. **Puneet Srivastava:** Conceptualization, Methodology, Funding acquisition, Writing-review, Supervision. **Jasmeet Lamba:** Funding acquisition, Conceptualization, Writing - review, Supervision. **Ryan P. McGehee:** Methodology, Formal analysis, Data curation, Writing - review & editing, Visualization. **Hemendra Kumar:** Conceptualization, Methodology. **Di Tian:** Writing - review, Data curation.

Data availability

Data will be made available on request.

Declaration of competing interest

The authors declare that they have no known competing financial interests or personal relationships that could have appeared to influence the work reported in this paper.

Acknowledgements

This work was completed in part with resources provided by the Auburn University Hopper Cluster. We are grateful for the support of USDA-NIFA Hatch Project (ALA014-1-19052), and the Alabama Agricultural Experiment Station funded this study. Additionally, we would like to express our appreciation to the editor (Manuel Esteban Lucas-Borja) and anonymous reviewers for their suggestions, which helped to improve the manuscript.

Appendix A. Supplementary file

Supplementary data to this article can be found online at https://doi.org/10.1016/j.scitotenv.2022.161119.

References

Allan, R.P., Soden, B.J., 2008. Atmospheric warming and the amplification of precipitation extremes. Science 321, 1481–1484. https://doi.org/10.1126/science.1160787.

Almagro, A., Oliveira, P.T.S., Nearing, M.A., Hagemann, S., 2017. Projected climate change impacts in rainfall erosivity over Brazil. Sci. Rep. 7, 8130. https://doi.org/10.1038/s41598-017-08298-y.

Ballabio, C., Borrelli, P., Spinoni, J., Meusburger, K., Michaelides, S., Beguería, S., Klik, A., Petan, S., Janeček, M., Olsen, P., Aalto, J., Lakatos, M., Rymszewicz, A., Dumitrescu, A., Tadić, M.P., Diodato, N., Kostalova, J., Rousseva, S., Banasik, K., Alewell, C., Panagos, P., 2017. Mapping monthly rainfall erosivity in Europe. Sci. Total Environ. 579, 1298–1315. https://doi.org/10.1016/j.scitotenv.2016.11.123.

Beguería, S., Serrano-Notivoli, R., Tomas-Burguera, M., 2018. Computation of rainfall erosivity from daily precipitation amounts. Sci. Total Environ. 637–638, 359–373. https://doi.org/10.1016/j.scitotenv.2018.04.400.

Biasutti, M., Seager, R., 2015. Projected changes in US rainfall erosivity. Hydrol. Earth Syst. Sci. 19, 2945–2961. https://doi.org/10.5194/hess-19-2945-2015.

Bonilla, C.A., Vidal, K.L., 2011. Rainfall erosivity in Central Chile. J. Hydrol. 410, 126–133. https://doi.org/10.1016/j.jhydrol.2011.09.022.

Borrelli, P., Robinson, D.A., Fleischer, L.R., Lugato, E., Ballabio, C., Alewell, C., Meusburger, K., Modugno, S., Schütt, B., Ferro, V., Bagarello, V., Oost, K.V., Montanarella, L., Panagos, P., 2017. An assessment of the global impact of 21st century land use change on soil erosion. Nat. Commun. 8, 2013. https://doi.org/10.1038/s41467-017-02142-7.

Borrelli, P., Alewell, C., Alvarez, P., Anache, J.A.A., Baartman, J., Ballabio, C., Bezak, N., Biddoccu, M., Cerdà, A., Chalise, D., Chen, S., Chen, W., De Girolamo, A.M., Gessesse, G.D., Deumlich, D., Diodato, N., Efthimiou, N., Erpul, G., Fiener, P., Freppaz, M., Gentile, F., Gericke, A., Haregeweyn, N., Hu, B., Jeanneau, A., Kaffas, K., Kiani-Harchegani, M., Villuendas, I.L., Li, C., Lombardo, L., López-Vicente, M., Lucas-Borja, M.E., Märker, M., Matthews, F., Miao, C., Mikoš, M., Modugno, S., Möller, M., Naipal, V., Nearing, M., Owusu, S., Panday, D., Patault, E., Patriche, C.V., Poggio, L., Portes, R., Quijano, L., Rahdari, M.R., Renima, M., Ricci, G.F., Rodrigo-Comino, J., Saia, S., Samani, A.N., Schillaci, C., Syrris, V., Kim, H.S., Spinola, D.N., Oliveira, P.T., Teng, H., Thapa, R., Vantas, K., Vieira, D., Yang, J.E., Yin, S., Zema, D.A., Zhao, G., Panagos, P., 2021. Soil erosion modelling: a global review and statistical analysis. Sci. Total Environ. 780, 146494. https://doi.org/10.1016/j.scitotenv.2021.146494.

Brown, L., Foster, G., 1987. Storm erosivity using idealized intensity distributions. Trans. ASAE 30, 379–386.

Cerdà, A., Flanagan, D.C., le Bissonnais, Y., Boardman, J., 2009. Soil erosion and agriculture. Soil Tillage Res. 106, 107–108. https://doi.org/10.1016/j.still.2009.10.006.

Chen, H., Sun, J., Lin, W., Xu, H., 2020. Comparison of CMIP6 and CMIP5 models in simulating climate extremes. Sci. Bull. 65, 1415–1418. https://doi.org/10.1016/j.scib.2020.05.015.

Chen, Y., Duan, X., Zhang, G., Ding, M., Lu, S., 2022. Rainfall erosivity estimation over the Tibetan Plateau based on high spatial-temporal resolution rainfall records. Int. Soil Water Conserv. Res. https://doi.org/10.1016/j.iswcr.2022.01.004.

Coles, S., Bawa, J., Trenner, L., Dorazio, P., 2001. An Introduction to Statistical Modeling of Extreme Values. Springer.

NOAA NCEI (National Oceanic and Atmospheric Administration, National Centers for Environmental Informationcollab, 2014. US 15 Minute Precipitation Data, Version 1.0. 1970-2010.

Easterling, D.R., Arnold, J.R., Knutson, T., Kunkel, K.E., LeGrande, A.N., Leung, L.R., Vose, R.S., Waliser, D.E., Wehner, M.F., 2017. Ch. 7: precipitation change in the United States. Climate Science Special Report: Fourth National Climate Assessment. volume I. U.S. Global Change Research Program. https://doi.org/10.7930/J0H993CC.

FAO, Clara, Ronald, 2019. Soil Erosion: The Greatest Challenge for Sustainable Soil Management Rome.

Fick, S.E., Hijmans, R.J., 2017. WorldClim 2: new 1-km spatial resolution climate surfaces for global land areas. Int. J. Climatol. 37, 4302–4315. https://doi.org/10.1002/joc.5086.

Fischer, F.K., Winterrath, T., Auerswald, K., 2018. Temporal- and spatial-scale and positional effects on rain erosivity derived from point-scale and contiguous rain data. Hydrol. Earth Syst. Sci. 22, 6505–6518. https://doi.org/10.5194/hess-22-6505-2018.

Flanagan, D.C., McGehee, R.P., Srivastava, A., 2020. Evaluation of different precipitation inputs to WEPP. 2020 ASABE Annual International Virtual Meeting, July 13-15, 2020. Presented at the 2020 ASABE Annual International Virtual Meeting, July 13-15, 2020. American Society of Agricultural and Biological Engineers https://doi.org/10.13031/aim.202000740.

Giorgi, F., Anyah, R.O., 2012. The road towards RegCM4. Clim. Res. 52, 3–6. https://doi.org/10.3354/cr01089.

Grillakis, M.G., Polykretis, C., Alexakis, D.D., 2020. Past and projected climate change impacts on rainfall erosivity: advancing our knowledge for the eastern Mediterranean island of Crete. Catena 193, 104625. https://doi.org/10.1016/j.catena.2020.104625.

Hollinger, S.E., Angel, J.R., Palecki, M.A., 2002. Spatial Distribution, Variation, and Trends in Storm Precipitation Characteristics Associated With Soil Erosion in the United States (No. ISWS Contract Report CR-2002-08). Illinois State Water Survey Circular.

Hoomehr, S., Schwartz, J.S., Yoder, D.C., 2016. Potential changes in rainfall erosivity under GCM climate change scenarios for the southern Appalachian region, USA. In: Lei, T.W., Yu, X.X., Zhuang, J. (Eds.), CATENA, Section 1: Special Issue on Reclamation of Mining Site Soils, Part I; Edited by: Jaume Bech. and Section 2 : Special Issue on Understanding Hydrological and Erosion Processes Under Changing Environment. 136, pp. 141–151. https://doi.org/10.1016/j.catena.2015.01.012.

Ingram, K., Dow, K., Carter, L., Anderson, J., 2013. Climate of the Southeast United States: Variability, Change, Impacts, and Vulnerability. Island Press, Washington DC.

IPCC, 2018. Global Warming of 1.5°C: An IPCC Special Report on the impacts of global warming of 1.5°C above pre-industrial levels and related global greenhouse gas emission pathways, in the context of strengthening the global response to the threat of climate change, sustainable development, and efforts to eradicate poverty. Cambridge University Press, Cambridge, UK and New York, NY, USA https://doi.org/10.1017/9781009157940.

Kamruzzaman, M., Shahid, S., Islam, A.T., Hwang, S., Cho, J., Zaman, Md.A.U., Ahmed, M., Rahman, Md.M., Hossain, Md.B., 2021. Comparison of CMIP6 and CMIP5 model performance in simulating historical precipitation and temperature in Bangladesh: a preliminary study. Theor. Appl. Climatol. 145, 1385–1406. https://doi.org/10.1007/s00704-021-03691-0.

Karl, T.R., Knight, R.W., Easterling, D.R., Quayle, R.G., 1996. Indices of climate change for the United States. Bull. Am. Meteorol. Soc. 77, 279–292. https://doi.org/10.1175/1520-0477(1996)077<0279:IOCCFT>2.0.CO;2.

Keim, B.D., Fontenot, R., Tebaldi, C., Shankman, D., 2011. Hydroclimatology of the U.S. Gulf Coast under global climate change scenarios. Phys. Geogr. 32, 561–582. https://doi.org/10.2747/0272-3646.32.6.561.

Kim, J., Han, H., Kim, B., Chen, H., Lee, J.-H., 2020. Use of a high-resolution-satellite-based precipitation product in mapping continental-scale rainfall erosivity: a case study of the United States. Catena 193, 104602. https://doi.org/10.1016/j.catena.2020.104602.

Kinnell, P.I.A., 2010. Event soil loss, runoff and the universal soil loss equation family of models: a review. J. Hydrol. 385, 384–397. https://doi.org/10.1016/j.jhydrol.2010.01.024.

Knight, D.B., Davis, R.E., 2007. Climatology of tropical cyclone rainfall in the southeastern United States. Phys. Geogr. 28, 126–147. https://doi.org/10.2747/0272-3646.28.2.126.

Konapala, G., Mishra, A.K., Wada, Y., Mann, M.E., 2020. Climate change will affect global water availability through compounding changes in seasonal precipitation and evaporation. Nat. Commun. 11, 3044. https://doi.org/10.1038/s41467-020-16757-w.

Kumar, H., Srivastava, P., Ortiz, B.V., Morata, G., Takhellambam, B.S., Lamba, J., Bondesan, L., 2021. Field-scale spatial and temporal soil water variability in irrigated croplands. Trans. ASABE 64, 1277–1294. https://doi.org/10.13031/trans.14335.

Kumar, H., Srivastava, P., Lamba, J., Diamantopoulos, E., Ortiz, B., Morata, G., Takhellambam, B., Bondesan, L., 2022a. Site-specific irrigation scheduling using one-layer soil hydraulic properties and inverse modeling. Agric. Water Manag. 273, 107877. https://doi.org/10.1016/j.agwat.2022.107877.

Kumar, H., Srivastava, P., Lamba, J., Ortiz, B.V., Way, T.R., Sangha, L., Takhellambam, B.S., Morata, G., Molinari, R., 2022b. Within-field variability in nutrients for site-specific agricultural management in irrigated cornfield. J. Agric. Saf. Health 65, 865–880. https://doi.org/10.13031/ja.15042.

Kunkel, K.E., Stevens, L.E., Stevens, S.E., Sun, L., Janssen, E., Wuebbles, D., Ii, C.E.K., Fuhrman, C.M., Keim, B.D., Kruk, M.C., Billet, A., Needham, H., Schafer, M., Dobson, J.G., 2013. Regional Climate Trends and Scenarios for the U.S. National Climate Assessment (No. NESDIS 142-2). National Oceanic and Atmospheric Administration. National Oceanic and Atmospheric Administration.

Lewis, E., Pritchard, D., Villalobos-Herrera, R., Blenkinsop, S., McClean, F., Guerreiro, S., Schneider, U., Becker, A., Finger, P., Meyer-Christoffer, A., Rustemeier, E., Fowler, H.J., 2021. Quality control of a global hourly rainfall dataset. Environ. Model. Softw. 144, 105169. https://doi.org/10.1016/j.envsoft.2021.105169.

Li, J., Huo, R., Chen, H., Zhao, Y., Zhao, T., 2021. Comparative assessment and future prediction using CMIP6 and CMIP5 for annual precipitation and extreme precipitation simulation. Front. Earth Sci. 9.

Martel, J.-L., Brissette, F., Troin, M., Arsenault, R., Chen, J., Su, T., Lucas-Picher, P., 2022. CMIP5 and CMIP6 model projection comparison for hydrological impacts over North America. Geophys. Res. Lett. 49, e2022GL098364. https://doi.org/10.1029/2022GL098364.

McGehee, R., 2016. Development of Reliable Erosion Indices for Climate-informed Soil Conservation in the Southeastern United States. Auburn University.

McGehee, R., Srivastava, P., 2018. Benchmarking reliable erosion indices from quarter-hour station data for climate studies in the southeastern United States. J. Soil Water Conserv. 73, 363–376. https://doi.org/10.2489/jswc.73.4.363.

McGehee, R.P., Flanagan, D.C., Srivastava, P., 2020. WEPPCLIFF: a command-line tool to process climate inputs for soil loss models. J. Open Source Softw. 5, 2029.

McGehee, R.P., Flanagan, D.C., Srivastava, P., Nearing, M.A., 2021. Chapter 16 - rainfall erosivity: essential historical, conceptual, and practical perspectives for continued application. In: Rodrigo-Comino, J. (Ed.), Precipitation. Elsevier, pp. 373–394 https://doi.org/10.1016/B978-0-12-822699-5.00014-8.

McGehee, R.P., Flanagan, D.C., Srivastava, P., Engel, B.A., Huang, C.-H., Nearing, M.A., 2022. An updated isoerodent map of the conterminous United States. Int. Soil Water Conserv. Res. 10, 1–16. https://doi.org/10.1016/j.iswcr.2021.06.004.

McGregor, K., Mutchler, C., 1976. Status of the R factor in northern Mississippi. Soil Eros. Predict. Control 135–142.

McGregor, K.C., Bingner, R.L., Bowie, A.J., Foster, G.R., 1995. Erosivity index values for northern Mississippi. Trans. ASAE 38, 1039–1047. https://doi.org/10.13031/2013.27921.

Mearns, L., McGinnis, S., Korytina, D., Arritt, R., Biner, S., Bukovsky, M., Chang, H.-I., Christensen, O., Herzmann, D., Jiao, Y., Kharin, S., Lazare, M., Nikulin, G., Qian, M., Scinocca, J., Winger, K., Castro, C., Frigon, A., Gutowski, W., 2017. The NA-CORDEX Dataset. https://doi.org/10.5065/D6SJ1JCH.

Meusburger, K., Steel, A., Panagos, P., Montanarella, L., Alewell, C., 2012. Spatial and temporal variability of rainfall erosivity factor for Switzerland. Hydrol. Earth Syst. Sci. 16, 167–177. https://doi.org/10.5194/hess-16-167-2012.

Mirhosseini, G., Srivastava, P., Stefanova, L., 2013. The impact of climate change on rainfall Intensity–Duration–Frequency (IDF) curves in Alabama. Reg. Environ. Chang. 13, 25–33. https://doi.org/10.1007/s10113-012-0375-5.

Mondal, A., Khare, D., Kundu, S., 2016. Change in rainfall erosivity in the past and future due to climate change in the central part of India. Int. Soil Water Conserv. Res. 4, 186–194. https://doi.org/10.1016/j.iswcr.2016.08.004.

Naipal, V., Ciais, P., Wang, Y., Lauerwald, R., Guenet, B., Oost, K.V., 2018. Global soil organic carbon removal by water erosion under climate change and land use change during AD 1850–2005. Biogeosciences 15, 4459–4480. https://doi.org/10.5194/bg-15-4459-2018.

Nearing, M.A., 2001. Potential changes in rainfall erosivity in the U.S. with climate change during the 21st century. J. Soil Water Conserv. 56, 229–232.

Nyssen, J., Vandenreyken, H., Poesen, J., Moeyersons, J., Deckers, J., Haile, M., Salles, C., Govers, G., 2005. Rainfall erosivity and variability in the Northern Ethiopian highlands. J. Hydrol. 311, 172–187. https://doi.org/10.1016/j.jhydrol.2004.12.016.

O'Neal, M.R., Nearing, M.A., Vining, R.C., Southworth, J., Pfeifer, R.A., 2005. Climate change impacts on soil erosion in Midwest United States with changes in crop management. CATENA, Soil Erosion Under Climate Change: Rates, Implications and Feedbacks 61, 165–184. https://doi.org/10.1016/j.catena.2005.03.003.

Op de Hipt, F., Diekkrüger, B., Steup, G., Yira, Y., Hoffmann, T., Rode, M., 2018. Modeling the impact of climate change on water resources and soil erosion in a tropical catchment in Burkina Faso, West Africa. Catena 163, 63–77. https://doi.org/10.1016/j.catena.2017.11.023.

Panagos, P., Ballabio, C., Borrelli, P., Meusburger, K., Klik, A., Rousseva, S., Tadić, M.P., Michaelides, S., Hrabalíková, M., Olsen, P., Aalto, J., Lakatos, M., Rymszewicz, A., Dumitrescu, A., Beguería, S., Alewell, C., 2015. Rainfall erosivity in Europe. Sci. Total Environ. 511, 801–814. https://doi.org/10.1016/j.scitotenv.2015.01.008.

Panagos, P., Borrelli, P., Meusburger, K., Yu, B., Klik, A., Jae Lim, K., Yang, J.E., Ni, J., Miao, C., Chattopadhyay, N., Sadeghi, S.H., Hazbavi, Z., Zabihi, M., Larionov, G.A., Krasnov, S.F., Gorobets, A.V., Levi, Y., Erpul, G., Birkel, C., Hoyos, N., Naipal, V., Oliveira, P.T.S., Bonilla, C.A., Meddi, M., Nel, W., Al Dashti, H., Boni, M., Diodato, N., Van Oost, K., Nearing, M., Ballabio, C., 2017. Global rainfall erosivity assessment based on high-temporal resolution rainfall records. Sci. Rep. 7, 4175. https://doi.org/10.1038/s41598-017-04282-8.

Panagos, P., Borrelli, P., Matthews, F., Liakos, L., Bezak, N., Diodato, N., Ballabio, C., 2022. Global rainfall erosivity projections for 2050 and 2070. J. Hydrol. 610, 127865. https://doi.org/10.1016/j.jhydrol.2022.127865.

Pimentel, D., 2006. Soil erosion: a food and environmental threat. Environ. Dev. Sustain. 8, 119–137. https://doi.org/10.1007/s10668-005-1262-8.

Pruski, F.F., Nearing, M.A., 2002. Climate-induced changes in erosion during the 21st century for eight U.S. locations. Water Resour. Res. 38, 34-1–34-11. https://doi.org/10.1029/2001WR000493.

Renard, K.G., 1997. Predicting Soil Erosion by Water: A Guide to Conservation Planning With the Revised Universal Soil Loss Equation (RUSLE). United States Government Printing.

Renard, K.G., Freimund, J.R., 1994. Using monthly precipitation data to estimate the R-factor in the revised USLE. J. Hydrol. 157, 287–306. https://doi.org/10.1016/0022-1694(94)90110-4.

Riquetti, N.B., Mello, C.R., Beskow, S., Viola, M.R., 2020. Rainfall erosivity in South America: current patterns and future perspectives. Sci. Total Environ. 724, 138315. https://doi.org/10.1016/j.scitotenv.2020.138315.

Rodda, J.C., 1967. The rainfall measurement problem. IAHS Publ. No 78, pp. 215–231.

Rodda, J.C., Dixon, H., 2012. Rainfall measurement revisited. Weather 67, 131–136. https://doi.org/10.1002/wea.875.

Scinocca, J.F., Kharin, V.V., Jiao, Y., Qian, M.W., Lazare, M., Solheim, L., Flato, G.M., Biner, S., Desgagne, M., Dugas, B., 2016. Coordinated global and regional climate modeling. J. Clim. 29, 17–35. https://doi.org/10.1175/JCLI-D-15-0161.1.

Seager, R., Tzanova, A., Nakamura, J., 2009. Drought in the southeastern United States: causes, variability over the last millennium, and the potential for future hydroclimate change. J. Clim. 22, 5021–5045. https://doi.org/10.1175/2009JCLI2683.1.

Segura, C., Sun, G., McNulty, S., Zhang, Y., 2014. Potential impacts of climate change on soil erosion vulnerability across the conterminous United States. J. Soil Water Conserv. 69, 171–181. https://doi.org/10.2489/jswc.69.2.171.

Shiono, T., Ogawa, S., Miyamoto, T., Kameyama, K., 2013. Expected impacts of climate change on rainfall erosivity of farmlands in Japan. Ecol. Eng., Soil Bio- and Eco-Engineering: The Use of Vegetation to Improve Slope Stability 61, 678–689. https://doi.org/10.1016/j.ecoleng.2013.03.002.

Skamarock, W., Klemp, J., Dudhia, J., Gill, D., Barker, D., Wang, W., 2005. A Description of the Advanced Research WRF Version 2. UCAR/NCAR https://doi.org/10.5065/D6DZ069T.

Swain, S., Hayhoe, K., 2015. CMIP5 projected changes in spring and summer drought and wet conditions over North America. Clim. Dyn. 44, 2737–2750. https://doi.org/10.1007/s00382-014-2255-9.

Takhellambam, B.S., Srivastava, P., Lamba, J., McGehee, R.P., Kumar, H., Tian, D., 2022. Temporal disaggregation of hourly precipitation under changing climate over the Southeast United States. Sci. Data 9, 211. https://doi.org/10.1038/s41597-022-01304-7.

Trenberth, K.E., Dai, A., Rasmussen, R.M., Parsons, D.B., 2003. The changing character of precipitation. Bull. Am. Meteorol. Soc. 84, 1205–1218. https://doi.org/10.1175/BAMS-84-9-1205.

USDA-ARS, 2008. User's Reference Guide: Revised Universal Soil Loss Equation (RUSLE2). US Department of Agriculture, Washington, DC.

USDA-ARS, 2013. Science Documentation Revised Universal Soil Loss Equation Version 2. US Department of Agriculture, Washington, DC.

USGCRP, 2018. Impacts, Risks, and Adaptation in the United States: Fourth National Climate Assessment [WWW Document]. URL (accessed 2.23.21) https://nca2018.globalchange.gov/chapter/19.

van Vuuren, D.P., Riahi, K., 2011. The relationship between short-term emissions and long-term concentration targets. Clim. Chang. 104, 793–801. https://doi.org/10.1007/s10584-010-0004-6.

Webb, N.P., Van Zee, J.W., Karl, J.W., Herrick, J.E., Courtright, E.M., Billings, B.J., Boyd, R., Chappell, A., Duniway, M.C., Derner, J.D., Hand, J.L., Kachergis, E., McCord, S.E., Newingham, B.A., Pierson, F.B., Steiner, J.L., Tatarko, J., Tedela, N.H., Toledo, D., Scott Van Pelt, R., 2017. Enhancing wind erosion monitoring and assessment for U.S. rangelands. Rangelands 39, 85–96. https://doi.org/10.1016/j.rala.2017.04.001.

Wischmeier, W.H., Smith, D.D., 1958. Rainfall energy and its relationship to soil loss. Trans. Am. Geophys. Union 39, 285. https://doi.org/10.1029/TR039i002p00285.

Wischmeier, W.H., Smith, D.D., 1965. Predicting Rainfall-erosion Losses From Cropland East of the Rocky Mountains (No. USDA Agricultural Handbook No. 282). USDA, Washington, DC.

Wischmeier, W.H., Smith, D.D., 1978. Predicting Rainfall Erosion Losses: A Guide to Conservation Planning. Department of Agriculture, Science and Education Administration.

Zhang, Y.-G., Nearing, M.A., Zhang, X.C., Xie, Y., Wei, H., 2010. Projected rainfall erosivity changes under climate change from multimodel and multiscenario projections in Northeast China. J. Hydrol. 384, 97–106. https://doi.org/10.1016/j.jhydrol.2010.01.013.

Zhao, W., Kinouchi, T., Nguyen, H.Q., 2021. A framework for projecting future intensity-duration-frequency (IDF) curves based on CORDEX Southeast Asia multi-model simulations: an application for two cities in southern Vietnam. J. Hydrol. 598, 126461. https://doi.org/10.1016/j.jhydrol.2021.126461.

Zhu, D., Xiong, K., Xiao, H., 2021. Multi-time scale variability of rainfall erosivity and erosivity density in the karst region of southern China, 1960–2017. Catena 197, 104977. https://doi.org/10.1016/j.catena.2020.104977.